Effect of Regular Anisotropic Permanent Bending on the Diffusional Spinning and Fluorescence Polarization Anisotropy of Short DNA Fragments Studied by Brownian Dynamics Simulation

Stuart A. Allison*

Department of Chemistry, Georgia State University, Atlanta, Georgia 30303

J. Michael Schurr

Department of Chemistry, Box 351700, University of Washington, Seattle, Washington 98195-1700

Received June 13, 1997; Revised Manuscript Received August 26, 1997[⊗]

ABSTRACT: The effects of regular permanent bends on the rotational Brownian motions of flexurally and torsionally deformable DNA models are investigated by Brownian dynamics simulations. Directionality of the permanent bends is maintained by anisotropic bending terms in the intersubunit potential. The effects of such bends on the effective hydrodynamic radius for diffusional spinning and on the fluorescence polarization anisotropy (FPA) are determined by comparing simulated results for three different model potentials: (1) a uniform isotropic bending potential with a straight resting geometry (I-model); (2) a uniform isotropic plus anisotropic permanent bending potential, which has the same average projection of a bond vector onto its predecessor as the I-model and which exhibits regular permanent bends (A-model); and (3) a mostly isotropic model, but with a single 90° anisotropic permanent bend at its center (L-model). A 72 base pairs (bp) I-model exhibits practically the same hydrodynamic radius for azimuthal spinning as the corresponding straight cylinder, whereas the A-model exhibits a slightly (3%) larger value over a range of filament lengths. The large directional permanent bend of the L-model substantially increases the hydrodynamic radius for diffusional spinning. However, when the anisotropic bending potential is omitted from either the A- or L-models, the permanent bends become nondirectional and have no significant effect on diffusional spinning, which evidently takes place via a uniform speedometer cable rotation. The FPA of the A-model indicates significantly less depolarization than is obtained for the I-model at any given time. The A-model FPA curves can be satisfactorily reproduced by suitably parametrizing the I-model so that (1) the effective hydrodynamic radius for azimuthal rotation is increased to emulate the effect of permanent bends; (2) the dynamic bending rigidity is chosen to emulate the short-time bending amplitude of the A-model; and (3) the rotational diffusion coefficient for end-over-end tumbling is chosen to reflect the total persistence length, including the effect of permanent bends.

Introduction

The Brownian torsional and flexural dynamics of DNA have been investigated extensively both theoretically and experimentally over the last 20 years.[1] Such studies have ascertained the time scales, approximate amplitudes, and scaling laws for such motions and yielded numerical estimates of the *dynamic* torsional and bending rigidities and hydrodynamic radii that govern those. Information regarding the *static*, or *equilibrium*, torsional and bending rigidities has come from parallel studies of equilibrium properties of linear and small circular DNAs, namely, the persistence length (P), free energy difference between topoisomers, and variation of cyclization free energy with length.[2−4]

Originally, DNA was imagined to behave as a uniform isotropic elastic cylinder with a fixed length, a straight resting geometry, and robust time-independent elastic constants. For this simplest model, which is henceforth denoted as model I, the persistence length (P) is related to the bending rigidity (A) by $P = A/k_BT$, where T is absolute temperature and k_B is Boltzmann's constant.[5]

As our knowledge of DNA has grown, our picture of DNA has evolved considerably in ways that significantly complicate the interpretations of both equilibrium and dynamical experiments on all DNAs longer than about 30 base pairs (bp). Sequence-dependent permanent bends are now believed to contribute significantly to the inverse total persistence length ($1/P_{tot}$).[6] Also, a variety of evidence, reviewed in Appendix B, suggests that the secondary structure of DNA neither resides nor thermally deforms exclusively within a single potential-of-mean-force, or free energy, basin but instead (for at least part of the sequence) may fluctuate between different basins. These basins correspond to different minimum free energy structures that may exhibit different twisting and bending rigidities, and the rate of equilibration between such basins is sometimes exceedingly slow.[7−11] In such a case, thermal fluctuations away from the average structure exhibit a fast component of relaxation due to Brownian deformations within the instantaneously prevailing free energy basins and a slower component due to net transfer of populations between such basins. The inverse total persistence length is now given approximately by[6]

$$\frac{1}{P_{tot}} \approx \frac{1}{P_{pb}} + \frac{1}{P_{sr}} + \frac{1}{P_d} \qquad (1)$$

where P_{pb} is the contribution of sequence-dependent permanent bends, P_{sr} is the contribution of slowly relaxing bends associated with slow conformational equilibria, and $P_d = A_d/k_BT$ is related to the single-basin dynamic bending rigidity (A_d) that governs the short-time dynamics. For $t \leq 1$ μs after the start of an

[⊗] Abstract published in *Advance ACS Abstracts,* November 1, 1997.

S0024-9297(97)00877-2 CCC: $14.00

experiment, the bending dynamics is governed mainly by a population-weighted average value of A_d (or P_d) for different basins, while the contributions of permanent and slowly relaxing bends are effectively "frozen" on that time scale. Experimental estimates range from P_d = 125 to 250 nm,[1,12−15] and the current best estimate for DNA in 0.1 M NaCl is P_d = 150 nm.[15] When the value P_d = 150 nm is adopted, the torsional rigidities obtained for small DNA circles ($N \leq 250$ bp) by time-resolved fluorescence polarization anisotropy (FPA) match those determined from topoisomer distributions,[7] while those obtained for linear and large circular DNAs[1,16] predict (via Monte Carlo simulations) supercoiling free energies, structure factors, and translational diffusion coefficients in good agreement with experiments on p30δ.[17,18] Combining P_d = 150 nm with the estimate of Schellman and Harvey, P_{pb} = 137 nm,[6] and P_{tot} = 50 nm yields $P_{sr} \approx$ 166 nm, which makes the three contributions to $1/P_{tot}$ roughly comparable.

On the time scale of a typical dynamics experiment, $t \leq 1$ μs, the *effectively* frozen or static bends make an estimated contribution, $1/P_{pb} + 1/P_{sr} = 1/137 + 1/166 = 1/75$ nm^{-1}, to the persistence length of DNA. Thus, during the short-time dynamics each DNA molecule relaxes toward a curved, rather that a straight, "resting" state, which should differ from one molecule to another due to the variable contribution of slowly relaxing bends. The main question addressed in the present study is how such frozen bends affect not only the apparent hydrodynamic radius (R_H) of the diffusional spinning motion but also the decay of the fluorescence polarization anisotropy (FPA).

There is an important difference between a molecule with such frozen bends and one with an isotropic bending potential (and straight resting geometry) that is instantaneously bent to the same degree. In particular, the latter molecule can undergo a uniform speedometer cable rotation, in which all subunits rotate in phase about their *fixed* symmetry axes, *while maintaining constant bending potential energy*, whereas the former molecule cannot. Such a motion is directly analogous to the spinning of a speedometer cable inside its stationary bent sheath or a plumbing snake in a stationary bent pipe. When a filament with (directional) frozen bends is forced to undergo such a uniform speedometer cable motion in which the local filament axis remains everywhere fixed, the potential energy varies with the phase of the speedometer cable rotation. Consequently, the frozen bends will to some extent become phase-locked to the uniform spinning motion in solution and thereby lend it some rigid-body crankshaft character. Because the filament arcs are displaced from the local spinning axis in such a crankshaft rotation, the fluid displacement and energy dissipation are greater than those for the corresponding speedometer cable motion. Consequently, the effective hydrodynamic radius for such motions is expected to somewhat exceed that for the corresponding straight filament. In contrast, the bends of an instantaneously bent filament with isotropic bending potential (and straight resting geometry) are *not* phase-locked to the uniform spinning motion, which then takes place in speedometer cable fashion. In this case, the effective hydrodynamic radius for uniform spinning should be nearly identical with the actual filament radius.[19] This conclusion, for which there already exists some evidence,[19,20] is further tested by Brownian dynamics and reaffirmed in the present work.

The case of completely rigid frozen filaments with random bends corresponding to P_{tot} = 50 nm (and also other values) was treated by Collini et al.,[21] who found that the effective hydrodynamic radius (R_H) for the uniform "spinning" of such nondeformable bent species increased substantially and progressively above the filament radius (R_o) with increasing contour length. Their work overestimates, and thus provides firm upper bounds for, the increase in R_H due to frozen (permanent plus slowly relaxing) bends. However, because real DNAs are flexible, dynamic deformations at (or near) constant potential energy will always facilitate some quasi-speedometer cable rotation that is considerably less eccentric than the uniform spinning of completely rigid bent species. Hence, the effective R_H of a real DNA is expected to rise less rapidly with increasing length than in the case for rigid-body crankshaft rotations. Moreover, some experimental evidence suggests that the increase in R_H due to permanent bends might not continue upward indefinitely but instead reaches a plateau value for lengths greater than about 170 bp.[19] For example, in most previous analyses of experimental FPA data, it appears that R_H is constant, independent of the length scales that are sampled over different time spans.[1]

The principal objective of the present work is to assess the effects of *regular* permanent bends on both R_H and the FPA of a flexible DNA model by Brownian dynamics simulation. The effects of *random* permanent bends, which require modeling an ensemble of variously bent molecules, will be addressed in subsequent work. For comparison, the effects of a single localized 90° bend are also investigated here. These theoretical results are intended to guide the interpretation of FPA experiments on DNAs of various lengths that have been, and are currently being, undertaken in an attempt to ascertain both the dynamic persistence length, $P_d = A_d/k_BT$, and the limiting value of R_H for long DNA segments, if such a limit actually exists.[22,23] In those experiments, for any choice of $P_d \geq 50$ nm, R_H equals 1.00 ± .01 nm for 12 and 24 bp DNAs but then rises for longer length fragments. The existing data rule out any P_d value less than about 100 nm but do not yet specify P_d more precisely, in part because R_H has evidently not reached its putative plateau value by 72 bp.[23] An important question is whether R_H actually exhibits plateau behavior with increasing length, and at what length that plateau is reached. A second important question is whether, and how closely, an appropriately parametrized isotropic model with suitable values of the various parameters, including P_d, the end-over-end rotational diffusion constant ($D_\perp$), and the value of R_H that governs the spinning diffusion constant (D_s^0), is able to fit simulated data for the model with permanent bends. Although a final answer to the former question must await similar studies on ensembles of models with random anisotropic permanent bends, the latter question is affirmatively answered by the present results.

Brownian dynamics simulations[12,24−31] have complemented the analytical theory used to analyze experimental FPA and other data for linear[1,27,30,32−38] and circular[20] DNAs by providing benchmark tests and verifying particular assumptions.[20,25−27,30] More importantly, Brownian dynamics simulations allow one to model such features as permanent bends and anisotropic bending,[12] for which satisfactory analytical theories are altogether lacking.

The plan of the paper is as follows. A rather general model, which comprises all of the particular models treated herein, is described along with its associated potential energy, which contains both isotropic and anisotropic permanent bending contributions. Anisotropy of the bending potential serves to orient the permanent bend in a particular direction, which is required for phase-locking of the bend to the uniform spinning motion. Next, the Brownian dynamics algorithm is detailed. The forces and torques employed are derived in a new way and presented in Appendix A. The selection of the common parameters, such as subunit size, hydrodynamic radii, average projection of a virtual bond onto its neighbor, stretching force constant, and torsional rigidity, is described next. Then, the particular parameters of the three models under consideration, namely, the isotropic (I) model, the regular anisotropic permanent bending (A) model, and the single large permanent bend (L) model, are detailed. The connection between simulated and analytical FPA results is discussed at the end of the Methods section. Simulated values of the spinning diffusion constants for the three models are presented and compared for DNAs of different lengths in the Results section. The predicted FPA decays for 72 bp I- and A-models are also presented and analyzed using the analytical theory, which applies for I-models. When the I-model is appropriately parametrized, so as to apply to a hybrid model (H), in which P_d and P_{tot} are allowed to differ, and the effective R_H may exceed the actual filament radius, a reasonably good fit to the A-model is obtained with very plausible values of the parameters.

Methods

General Model and Potential of Mean Force. The linear chain model used here is similar to that employed previously[12] except for differences in the bending potential to be discussed shortly. The chain is modeled as N identical rigid beads of radius a connected by $N-1$ virtual bonds, or rodlets. Let $\mathbf{r}_i$ denote the position of the center of bead i in the laboratory frame of reference and $b_i = |\mathbf{r}_{i+1} - \mathbf{r}_i|$ be the length of rodlet i. Since we are interested in a model which accounts for torsional strain as well as anisotropic bending of the chain, there are more than $3N$ coordinates (the $\mathbf{r}_i$'s) required to uniquely define the chain. It is useful to identify $N-1$ local, body-fixed reference frames associated with the rodlets and call these Σ_1 through Σ_{N-1}. Let $\mathbf{u}_i = (\mathbf{r}_{i+1} - \mathbf{r}_i)/b_i$ denote a unit vector along rodlet i and choose the z-axis of Σ_i to lie along $\mathbf{u}_i$. In the limit of a continuous wormlike chain model, $\mathbf{u}_i$ represents the tangent vector to the chain. At right angles to $\mathbf{u}_i$, define vector $\mathbf{f}_i$ which is chosen to lie along the x-axis of Σ_i. Physically, $\mathbf{f}_i$ might point in the direction of the local major groove if we are modeling DNA. It is helpful to view the $N-1$ rodlets as rectangles or ribbons. The long axis of ribbon i points along $\mathbf{u}_i$ and the short axis points along $\mathbf{f}_i$.[12] The relative positions of the **f**-vectors play an essential role in chain dynamics when torsional strain and/or anisotropic bending is important. Finally, we choose $\mathbf{v}_i$ to lie along the y-axis of (right-handed) reference frame Σ_i. It is uniquely determined once $\mathbf{f}_i$ and $\mathbf{u}_i$ are defined.

A total of $4N-1$ generalized coordinates are required to uniquely define the chain. We could, for example, choose three of these generalized coordinates to correspond to the three Cartesian components of bead 1 in the laboratory frame, $\mathbf{r}_1$. Let $\Phi_{L1} = (\alpha_L, \beta_L, \gamma_L)$ represent the three Euler angles that transform the lab frame into Σ_1 (i.e., carry a coordinate frame coincident with the lab frame into one coincident with Σ_1). This also serves to define $\{\mathbf{f}_1, \mathbf{v}_1, \mathbf{u}_1\}$ in the lab frame. Next specifying b_1 determines $\mathbf{r}_2$. To determine $\mathbf{r}_3$ as well as $\mathbf{f}_2$ requires the specification of three Euler angles, $\Phi_{1,2} = (\alpha_1, \beta_1, \gamma_1)$ which transform Σ_1 into Σ_2 as well as b_2. This process is repeated until $\mathbf{r}_N$ is finally specified by $\Phi_{N-2,N-1}$ and b_{N-1}. In the present work, the potential energy of the chain is independent of the overall position or orientation and so will depend on $4N-7$ variables. We can identify these as the $N-1$ rodlet lengths, b_i ($i = 1$ to $N-1$), and the $3(N-2)$ Euler angles, $(\alpha_i, \beta_i, \gamma_i)$ ($i = 1$ to $N-2$). For any virtual displacement of the chain, we can write the change in potential energy, δU, as

$$\delta U = \sum_{i=1}^{N-1}\left(\frac{\partial U}{\partial b_i}\right)\delta b_i + \sum_{i=1}^{N-2}\left[\left(\frac{\partial U}{\partial \alpha_i}\right)\delta\alpha_i + \left(\frac{\partial U}{\partial \beta_i}\right)\partial\beta_i + \left(\frac{\partial U}{\partial \gamma_i}\right)\delta\gamma_i\right] \tag{2}$$

Equation 2 is important in defining the forces on the beads and the torques on the rodlets as discussed in Appendix A.

The potential energy of our linear chain is assumed to have the form

$$U = U^s + U^t + U^b \tag{3}$$

where s, t, and b denote stretching, twisting, and bending components, respectively. In simulations of circular DNAs, it is also important to put in excluded volume/electrostatic repulsion terms as well[29,31] since these are important to prevent "strand passage" in supercoiled DNAs. For short linear DNAs, however, these terms are not important so they are neglected here. The stretching and twisting terms are

$$\frac{U^s}{k_B T} = \frac{1}{2}\sum_{j=1}^{N-1} c\left(\frac{b_j}{b} - 1\right)^2 \tag{4}$$

$$\frac{U^t}{k_B T} = \frac{1}{2}\sum_{j=1}^{N-2} q(\alpha_j + \gamma_j - \phi_0)^2 \tag{5}$$

where k_B is Boltzmann's constant, T is absolute temperature, c and q are dimensionless force constants for respectively stretching and twisting (assumed to be uniform throughout the chain in this work), b represents the position of the minimum in the stretching potential, and ϕ_0 represents the intrinsic twist angle between adjacent rodlets. A simple rodlet potential which exhibits anisotropic bending is given by[39]

$$\frac{U'}{k_B T} = \frac{1}{2} g\beta^2(\cos^2 x + \rho \sin^2 x) \tag{6}$$

where $x = (\alpha - \gamma - \psi_0)$, g is a (dimensionless) bending force constant, ρ (≥ 1.0) is the "bending anisotropy parameter", and ψ_0 is a constant angle that orients the "easy" bending directions. The total potential energy must be the same whether expressed in terms of the Euler angles, $\Phi_{j,j+1}$, for advancing forward from j to $j+1$, or in terms of the $\Phi_{j+1,j} = \Phi_{j,j+1}^{-1}$ for retreating backward from $j+1$ to j, when the coordinate frame vectors $\{\mathbf{f}_j, \mathbf{v}_j, \mathbf{u}_j\}$ are held fixed. The values of ϕ_0, ψ_0, and the intrinsic bend, β_0, that apply when advancing forward become $-\phi_0$, $-\psi_0$, and $-\beta_0$, respectively, when retreating backward. Thus, the total potential energy must be invariant to the transformation $\{\alpha_j, \beta_j, \gamma_j; \phi_0, \beta_0, \psi_0\} \rightarrow \{-\gamma_j, -\beta_j, -\alpha_j; -\phi_0, -\beta_0, -\psi_0\}$. The twisting potential and anisotropic bending potential given above satisfy this condition, as does the overall bending potential given below. According to the elliptical potential in eq 6, the rodlet exhibits an effective force constant of either g or ρg for bending in the azimuthal direction $x = 0$ or $\pi/2$, respectively. Although eq 6 admits anisotropic bending, it does not allow for the existence of permanent bends or the variation in bending parameters along the chain. In order to incorporate

these features, the following bending potential is used instead of U' in eq 6:

$$\frac{U^{\mathrm{b}}}{k_{\mathrm{B}}T} = \frac{1}{2}\sum_{j=1}^{N-2}[g_j(\beta j - \beta_{j0})^2 + p_j\beta_j{}^2(\alpha_j - \gamma_j - \psi_{j0})^2] = \frac{U^{\mathrm{bi}}}{k_{\mathrm{B}}T} + \frac{U^{\mathrm{ba}}}{k_{\mathrm{BT}}} \quad (7)$$

where U^{bi} is an isotropic bending potential for displacements away from the angle (β_{j0}) of intrinsic bend, U^{ba} is an anisotropic bending potential, g_j and p_j are isotropic and anisotropic bending force constants (which may vary along the chain), and ψ_0 is an intrinsic angle that specifies the direction of the permanent bend. In the absence of the second term, the intrinsic bends β_{j0} would not be phase-locked to the azimuthal spinning motion. Also, the anisotropic bending potential, U^{ba}, is noncentrosymmetric, because it is not invariant under the transformation $\alpha - \gamma \rightarrow \alpha - \gamma + \pi$. Consequently, at any finite temperature, it contributes an *average* directional permanent bend. Thus, in this model, the average extent of directional permanent bending at 293 K contains contributions from both U^{bi} and U^{ba}. If we set $\beta_{j0} = 0$, expand the cos and sin terms in eq 6, and keep the leading terms in x, we can identify p_j with $g_j(\rho_j - 1)$. Thus, the case $p_j \approx g_j$ corresponds to a virtual bond (rodlet) that is about twice as stiff to bend in the direction $x = \pi/2$ as in the direction $x = 0$.

Brownian Dynamics. As discussed in a paper by Heath et al.,[20] hereafter referred to as paper I, a particular Brownian dynamics (BD) step of duration Δt is divided into two substeps. In the first substep, the subunits are fixed in position and the rodlets are allowed to rotate about their local z-axes. Let $\delta R_{zi}(\Delta t)$ denote the rotational displacement of rodlet i in the first substep. A first-order BD displacement is given by

$$\delta R_{zi}(\Delta t) = \frac{D_{\mathrm{R}}}{k_{\mathrm{B}}T}\Delta t T_i(t) + \theta_i(\Delta t) \quad (8)$$

where D_{R} is the rotational diffusion constant of the rodlet, $T_{\mathrm{i}}(t)$ is the instantaneous torque at the beginning of the step (time = t), and $\theta_i(\Delta t)$ is a Gaussian random number of zero mean and variance−covariance

$$\langle \theta_i(\Delta t)\, \theta_j(\Delta t)\rangle = 2D_{\mathrm{R}}\Delta t\, \delta_{ij} \quad (9)$$

where δ_{ij} is the Kronecker delta. For eq 8 to be valid, Δt should be chosen small enough that the torques do not change significantly during such steps. Somewhat longer time steps can be taken if a second-order algorithm[29,40] is adopted. A more accurate equation of motion than eq 8 is

$$\delta R_{zi}(\Delta t) = \frac{D_{\mathrm{R}}\Delta t}{2k_{\mathrm{B}}T}[T_{\mathrm{i}}(t) + T_{\mathrm{i}}(t+\Delta t)] + \theta_i(\Delta t) \quad (10)$$

As it stands, however, eq 10 is impractical since the configuration-dependent quantity $T_{\mathrm{i}}(t+\Delta t)$ is unknown at the beginning of the time step. Instead, we first estimate the rotations, $\delta R_{zi}'(\Delta t)$, using first order eq 8 and then correct it according to

$$\delta R_{zi}(\Delta t) = \delta R_{zi}'(\Delta t) + \delta R_{zi}''(\Delta t) \quad (11)$$

where

$$\delta R_{zi}''(\Delta t) = \frac{D_{\mathrm{R}}\Delta t}{2k_{\mathrm{B}}T}[T_{\mathrm{i}}'(t+\Delta t) - T_{\mathrm{i}}(t)] \quad (12)$$

and $T_{\mathrm{i}}'(t+\Delta t)$ is evaluated at the intermediate chain configuration using the $\{\delta R_{zi}'(\Delta t)\}$. It can be shown that for small rotational displacements

$$\alpha_i' + \gamma_i' = \alpha_i + \gamma_i + \delta R_{zi+1}'(\Delta t) - \delta R_{zi}'(\Delta t) \quad (13)$$

Explicit expressions for the torques are given by eqs A5a−c in Appendix A.

After this substep, the $\mathbf{f}_i$ and $\mathbf{v}_i$ vectors change by

$$\delta\mathbf{f}_i = \delta R_{zi}\mathbf{v}_i \quad (14a)$$

$$\delta\mathbf{v}_i = -\delta R_{zi}\mathbf{f}_i \quad (14b)$$

and the resulting $\mathbf{f}_i$ and $\mathbf{v}_i$ vectors are renormalized.

In the second substep, the beads are allowed to translate according to the (first-order) Ermak−McCammon algorithm[41]

$$\mathbf{r}_i(t+\Delta t) = \mathbf{r}_i(t) + \frac{\Delta t}{k_{\mathrm{B}}T}\sum_{j=1}^{N}\mathbf{D}_{ij}(t)\cdot\mathbf{F}_j(t) + \mathbf{S}_i(\Delta t) \quad (15)$$

where $\mathbf{D}_{ij}(t)$ is the hydrodynamic interaction tensor between beads i and j, $\mathbf{F}_j(t)$ is the force on bead j at time t, and $\mathbf{S}_i(\Delta t)$ is a vector of Gaussian random numbers of zero mean and variance−covariance

$$\langle \mathbf{S}_i(\Delta t)\, \mathbf{S}_j(\Delta t)\rangle = 2\mathbf{D}_{ij}(t)\, \Delta t \quad (16)$$

Expressions for $\mathbf{D}_{ij}$ and procedures for generating the $\mathbf{S}_i$'s are described elsewhere.[25,26] Explicit expressions for the forces are given in eqs A15a−A24 in Appendix A. Although it is straightforward to employ a second-order algorithm[29,40] for this substep as well, it is our conclusion that no advantage is gained by a second-order algorithm under the parameter conditions employed in this work. Consequently, we have employed the simpler first-order algorithm for the second substep. Once the beads have been displaced, it is straightforward to update the $\mathbf{u}_i$'s. By constraining the rodlet rotations about their (initial) local z-axes to vanish during this substep, it was shown in paper I that

$$\delta\mathbf{f}_i = -(\delta\mathbf{u}_i\cdot\mathbf{f}_i)\mathbf{u}_i \quad (17a)$$

$$\delta\mathbf{v}_i = -(\delta\mathbf{u}_i\cdot\mathbf{v}_i)\mathbf{u}_i \quad (17b)$$

Once the unit vectors $\{\mathbf{f}_i, \mathbf{v}_i, \mathbf{u}_i\}$ and bond lengths have been determined after the complete BD step, it is necessary to compute the forces and torques for the next substep. As before, the β_i's are computed on the interval $(0, \pi)$ via

$$\beta_i = \arccos(\mathbf{u}_i\cdot\mathbf{u}_{i+1}) \quad (18)$$

Because of anisotropic bending and the problem associated with multivalued functions, determination of α_i and γ_i is done somewhat differently than in paper I. For a chain with a moderately stiff torsional force constant q, we expect $|\alpha_i + \gamma_i - \phi_0|$ to be fairly small. We first compute

$$c_1 = \cos(\alpha_i + \gamma_i - \phi_0) = \frac{(\mathbf{v}_i\cdot\mathbf{v}_{i+1} + \mathbf{f}_i\cdot\mathbf{f}_{i+1})\cos\phi_0 + (\mathbf{v}_i\cdot\mathbf{f}_{i+1} - \mathbf{f}_i\cdot\mathbf{v}_{i+1})\sin\phi_0}{1 + \mathbf{u}_i\cdot\mathbf{u}_{i+1}} \quad (19a)$$

$$s_1 = \sin(\alpha_i + \gamma_i - \phi_0) = \frac{(\mathbf{v}_i\cdot\mathbf{f}_{i+1} - \mathbf{f}_i\cdot\mathbf{v}_{i+1})\cos\phi_0 - (\mathbf{v}_i\cdot\mathbf{v}_{i+1} + \mathbf{f}_i\cdot\mathbf{f}_{i+1})\sin\phi_0}{1 + \mathbf{u}_i\cdot\mathbf{u}_{i+1}} \quad (19b)$$

We then compute $x_1 = \arccos(c_1)$ which gives x_1 on the interval $(0, \pi)$. However, if s_1 is negative, the sign of x_1 is changed.

Now equating x_1 with $\alpha_i + \gamma_i - \phi_0$ gives us $\alpha_i + \gamma_i - \phi_0$ on the interval $(-\pi, +\pi)$. Next we compute

$$c_2 = \cos(\alpha_i - \gamma_i - \psi_{i0}) = \frac{(\mathbf{v}_i\cdot\mathbf{v}_{i+1} - \mathbf{f}_i\cdot\mathbf{f}_{i+1})\cos\psi_{i0} - (\mathbf{f}_i\cdot\mathbf{v}_{i+1} + \mathbf{v}_i\cdot\mathbf{f}_{i+1})\sin\psi_{i0}}{1 - \mathbf{u}_i\cdot\mathbf{u}_{i+1}} \quad (20a)$$

$$s_2 = \sin(\alpha_i - \gamma_i - \psi_{i0}) = \frac{-(\mathbf{f}_i\cdot\mathbf{v}_{i+1} + \mathbf{v}_i\cdot\mathbf{f}_{i+1})\cos\psi_{i0} - (\mathbf{v}_i\cdot\mathbf{v}_{i+1} - \mathbf{f}_i\cdot\mathbf{f}_{i+1})\sin\psi_{i0}}{1 - \mathbf{u}_i\cdot\mathbf{u}_{i+1}} \quad (20b)$$

Following a procedure identical to that just considered, we generate a *tentative* $\alpha_i - \gamma_i - \psi_{i0}$, call it x_2, on the interval $(-\pi, +\pi)$. However, when $\beta_i \approx 0$, we cannot expect $\alpha_i - \gamma_i - \psi_{i0}$ to necessarily fall in this range. We can relate x_2 to the actual $\alpha_i - \gamma_i - \psi_{i0}$ by

$$x_2 = \alpha_i - \gamma_i - \psi_{i0} + 2\pi n \quad (21)$$

where n is an unknown integer. From eq 20 and the definition of x_1

$$\alpha_i = -\pi n + \alpha_i' \quad (22a)$$

$$\gamma_i = +\pi n + \gamma_i' \quad (22b)$$

where $\alpha_i' = (x_1 + x_2 + \phi_0 + \psi_{i0})/2$ and $\gamma_i' = (x_1 - x_2 + \phi_0 - \psi_{i0})/2$. Now

$$\sin\beta_i \cos\alpha_i = \mathbf{f}_i\cdot\mathbf{u}_{i+1} = (-)^n \cos\alpha_i' \sin\beta_i \quad (23)$$

If $x_3 = (\mathbf{f}_i\cdot\mathbf{u}_{i+1})/(\sin\beta_i \cos\alpha_i') \approx 1$, then n is even; but if $x_3 \approx -1$, then n is odd. This, however, is as far as one can go. If $x_3 \approx 1$, we simply set $n = 0$ (corresponding to that even n-value which minimizes U^{ba}). If $x_3 \approx -1$, we choose $n = +1$ or -1 depending on which choice minimizes U^{ba}. We have found that these precautions are necessary to insure that

$$\langle(\alpha_i + \gamma_i - \phi_0)^2\rangle \approx \frac{1}{q} \quad (24)$$

during a dynamics trajectory when a nonvanishing U^{ba} is present.

Selection of Chain Parameters. Our general objective is to model the conformational and dynamical behavior of a continuous deformable filament with contour length L, radius R, and various extents of directional anisotropic permanent bending by a corresponding discrete chain of practically contiguous spherical beads that are connected by springs with appropriate potential energy functions. Current consensus places the hydrodynamic radius for both azimuthal rotation and end-over-end tumbling of short (≤24 bp) DNAs at about $R = 1$ nm.[22,37,38,42,43] In our discrete model, the number (N) and radius (a) of the beads, and the subunit separation ($b = 2a$) that minimizes the stretching potential, are chosen according to the procedure of Hagerman,[44,45] so as to provide the same friction factors for end-over-end tumbling and translation as those for a straight cylinder of length L and radius $R = 1$ nm. One sets $L = Nb$, and the volume of the corresponding continuous wormlike chain ($\pi R^2 L$) is set equal to the volume of the bead array ($4\pi N a^3/3$). This gives $b = 2a = (6)^{1/2}R = 2.449$ nm. In other words, the two parameters N and a (or b) correspond to a particular L and R. While N spherical beads of radius $a = 1.224$ nm are employed to calculate the diffusion tensors appearing in eqs 15 and 16 of the translation substep of the Brownian dynamics algorithm, the $N - 1$ rodlets are regarded as small cylinders of radius $R = 1.00$ nm in order to calculate their rotational diffusion constant (D_R) that appears in eqs 10 and 12 of the azimuthal rotation substep. Before discussing the rodlet rotational diffusion coefficient D_R, consider the uniform "spinning diffusion constant" of the entire chain, which is defined by

$$D_s^0 = \lim_{t\to\infty} \frac{1}{2}\frac{d}{dt}\langle R_z(t)^2\rangle \quad (25)$$

where

$$R_z(t) = \frac{1}{N-1}\sum_{i=1}^{N-1} R_{zi}(t) \quad (26a)$$

$$R_{zi}(t+\Delta t) = R_{zi}(t) + \delta R_{zi}(\Delta t) \quad (26b)$$

and $\delta R_{zi}(\Delta t)$ is given by eq 11. At $t = 0$, $R_{zi}(t)$ is set to 0. In the special case of a short and stiff isotropic wormlike chain (g and q large and uniform, $p = 0$) with no permanent bends ($\beta_{i0} = 0$), D_s^0 should correspond to the diffusion constant of a cylinder of length L and radius R for rotation about its axis of symmetry, which is given by[46]

$$D_{cyl}^{\parallel} = \frac{k_B T}{3.841\pi\eta L R^2(1 + \delta_{\parallel})} \quad (27)$$

where $\delta_{\parallel}$ is an end correction factor tabulated elsewhere.[38,46] For a short stiff wormlike chain, by using eqs 8 and 9 in eqs 25 and 26, it is straightforward to show that $D_s^0 = D_R/(N - 1)$. Hence, we can write

$$D_R = \frac{k_B T}{4\pi\eta R^2 b_{eff}} \quad (28)$$

where

$$b_{eff} = \frac{0.9603L}{N-1}(1 + \delta_{\parallel}) \quad (29)$$

For a given contour length, D_R is calculated using eqs 28 and 29. For $N = 4$, 6, 8, 10, 15, and 20, $L = 9.796$, 14.694, 19.592, 24.490, 36.735, and 48.98 nm, respectively. The corresponding b_{eff}'s are 3.549, 3.076, 2.870, 2.757, 2.613, and 2.545 nm, respectively. The number of base pairs in a filament of a given contour length is taken to be $N_{bp} = L/h$ where $h = 0.34$ nm is the rise per bp along the helix axis.

The stretching force constant, c, is related to the rodlet (virtual bond) length moments through the relation

$$\langle b^m\rangle = \frac{\int_0^\infty x^{m+2} e^{-(c/2)((x/b)-1)^2}\,dx}{\int_0^\infty x^2 e^{-(c/2)((x/b)-1)^2}\,dx} \quad (30)$$

For large c, eq 30 yields $\langle b\rangle = b(1 + 1/c)$ and $\langle b^2\rangle = b^2(1 + 5/c)$. In the present work, we set $c = 1000$ throughout. This merely insures that the average or root-mean-square (rms) rodlet lengths lie close to b but at the same time does not force us to take inordinately short dynamics time steps. No attempt is made to match the stretching potential of the present model to that measured by Smith et al.[47]

Attention is now turned to the torsional or twisting parameters. At the present time, the torsional rigidity of *linear* DNAs, C, is estimated to lie between 1.70 and 2.30×10^{-19} erg cm.[7] The higher values obtained from topoisomer distributions and cyclization kinetics measurements on small circles with $N \leq 250$ bp, which have been widely employed in simulations of supercoiled DNAs, were recently shown to arise from perturbed secondary structure that is induced by the bending strain present in such small circles and are not applicable to linear and larger circular DNAs.[18] The torsional rigidity is related to the torsional force constant, q, by $C = k_B T\langle b\rangle q$. Choosing $q = 20.12$ gives $C = 1.99 \times 10^{-19}$ erg cm at 20 °C, and this value is used throughout this work. Also, DNA base pairs spiral through one complete turn (2π radians) in about 10 base pairs or 1.39 subunits. This corresponds to a

pitch angle, ϕ_0, of +4.52 rad. It is more convenient to deal with angles on the interval $(-\pi, +\pi)$, so instead we set $\phi_0 = 4.52 - 2\pi = -1.76$ rad.

For bending, the average projection of a virtual bond vector onto its neighbor is related to force constants in the bending potential by the relation

$$\langle \cos \beta_i \rangle = \frac{\int_0^\pi \sin(x) \cos(x) h_i(x)\, dx}{\int_0^\pi \sin(x) h_i(x)\, dx} \tag{31}$$

where

$$h_i(x) = \int_{-\pi}^{+\pi} d\nu\, e^{-(1/2)g_i(x-\beta_{i0})^2 - (1/2)p_i x^2 \nu^2} \tag{32}$$

is the distribution function for $x = \beta_i$. In general, eqs 31 and 32 must be integrated numerically for a particular choice of (g_i, p_i, β_{i0}). In the special case of isotropic bending ($p_i = 0$) and no permanent bends ($\beta_{i0} = 0$) a power series solution of eq 31 is possible. To order g^{-3} (omitting the i subscript), eq 31 reduces to

$$\langle \cos \beta \rangle \approx 1 - \frac{1}{g} + \frac{2}{3g^2} - \frac{14}{45g^3} \tag{33}$$

If g is also uniform along the entire chain, then the persistence length, P, can be related to g by the well known relation[6]

$$P = \frac{\langle b \rangle}{1 - \langle \cos \beta \rangle} \approx \frac{\langle b \rangle g}{1 - \frac{2}{3g} + \frac{14}{45g^2}} \tag{34}$$

For a particular P and $\langle b \rangle$, it is straightforward to solve eq 34 iteratively for g. If, for example, $P = 50$ nm, $b = 2.449$ nm, and $c = 1000$, it is straightforward to show $g = 19.74$. To approximate the dynamics of a completely rigid straight rod, one simply sets g to a large value.

In this work, the different simulated models fall into three main categories noted below. The same subunit size, diffusion constant for rodlet azimuthal rotation, stretching potential, and torsion potential are assumed to apply in all three models. However, their bending potentials differ, as follows.

(1) Isotropic Model (I). The I-models exhibit neither intrinsic bends nor anisotropic bending, so $\beta_{j0} = 0$ and $p_j = 0$ for all subunits. It is assumed that the bending rigidity is uniform along the chain and that $P = 50$ nm, so $g = 19.74$, as noted above. In this case, the average projection of one virtual bond onto its neighbor is $\langle \cos \beta \rangle = 0.951$.

(2) Anisotropic Permanent Bending Model (A). The bending potential of the A-models is assumed to be uniform along the filament and is chosen so that $\langle \cos \beta \rangle = 0.951$, as in the I-model. Because the bending potential of the A-model is uniform, its intrinsic bending is regular rather than random, and its resting geometry is therefore a (super) helix. Its persistence length has not yet been evaluated, although that could, in principle, be done by the protocol described previously for noncentrosymmetric potentials.[39] Since the permanent anisotropic bending in this model is regular, its contribution to $1/P_{tot}$ differs qualitatively from that of statistically random bends, in which case eq 1 might no longer apply. For this and other reasons, a comparison of isotropic and anisotropic models with the same $\langle \cos \beta \rangle$ is more relevant for our purposes than a comparison of such models with the same persistence length.

Unfortunately, there is little experimental information available to us on which to base our parametrization of g, p, and β_0 so our choices will be based on what we regard as plausible physical values for these parameters. Our main objective is to ascertain at a qualitative level what effect anisotropic bending and permanent bends have on the effective R_H and fluorescence polarization anisotropy of DNA. We feel that reasonable guesses of g, p, and β_0 will be able to tell us this. To begin, the three parameters are constrained to give the same value of $\langle \cos \beta \rangle = 0.951$ as the I-model with $P = 50$ nm. For nonvanishing β_0, we expect that g should be substantially larger than the corresponding isotropic value ($g = 19.74$). We simply set $g = 46.6$ which would correspond to a dynamic persistence length $P_d = 116$ nm (obtained by inserting this g-value in eq 34). This is in fairly good agreement with the best current estimate, $P_d = 150$ nm.[7,15] Also, p is set to 38.8 (which corresponds to $\rho = 1.83$). With these choices, $\beta_0 = 0.273$ rad (15.6°) is required to give the same $\langle \cos \beta \rangle = 0.951$ as the corresponding I-model. Throughout the remainder of this work, the anisotropic permanent bending model with the above choice of parameters will be called the A-model.

(3) Large Permanent Bend Model (L). This L-model has the same bending potential as the I-model, except that a 90° bend is placed in the middle of the chain. Specifically, for a 10-bead model, the bending potential for bonds 4 and 5 has $g = 100$, $p = 100$, $\psi_0 = 0$, and $\beta_0 = \pi/2$. For the remaining bonds, $g = 100$, $p = 0$, $\psi_0 = 0$, and $\beta_0 = 0$. In addition, the conformation of this model is basically "L" shaped.

Fluorescence Polarization Anisotropy. Over the last 20 years, fluorescence polarization anisotropy (FPA) of intercalated ethidium has been extensively used to explore the collective twisting and bending motions of DNA.[1,7−11,16,22,23,35−38] In addition to the overall and collective internal motions of DNA, the ethidium probe dye undergoes a rapid libration or "dye wobble" of small amplitude about its binding site. After this rapid isotropic dye wobble has relaxed, the emission anisotropy can be written as

$$r(t) = \frac{I_{||}(t) - I_{\perp}(t)}{I_{||}(t) + 2I_{\perp}(t)} = r_0 \langle P_2(\cos [\mathbf{d}(0) \cdot \mathbf{d}(t)]) \rangle \tag{35}$$

where r_0 is the diminished initial anisotropy,[36,37] P_2 is the second order Legendre polynomial, $\mathbf{d}(t)$ is a unit vector along the minimum energy orientation of the emission dipole of a particular bound ethidium at time t, and brackets denote an ensemble average over all bound dyes in all possible binding sites. Assume that there are $N - 1$ equivalent binding sites on the chain (corresponding to the $N - 1$ rodlets of the model employed in the present study). The FPA curves generated by Brownian dynamics are obtained by explicit calculation of eq 35 for several dye binding geometries. In order to make contact with the analytical theories,[32−34] however, more development is necessary. Making use of the properties of the Wigner rotation matrices and defining a reduced emission anisotropy, $r'(t) = r(t)/r_0$, eq 34 can be written as

$$r'(t) = \frac{1}{N-1} \sum_{i=1}^{N-1} \sum_{m,n=-2}^{+2} D^{2*}_{m0}(\Phi_d)\, D^2_{n0}(\Phi_d) \langle D^2_{mn}(\Phi_{it}) \rangle \tag{36}$$

where

$$D^L_{mn}(\Phi) = D^L_{mn}(\alpha,\beta,\gamma) = e^{-i(m\alpha + n\gamma)} d^L_{mn}(\beta) \tag{37}$$

is a Wigner rotation matrix element,[48,49] the asterisk denotes complex conjugation, $\Phi_d = (\upsilon, \epsilon, 0)$ where υ and ϵ are the azimuthal and polar angles, respectively, of the minimum energy orientation of the emission dipole with respect to local reference frame Σ_i, of rodlet i, Φ_{it} is the Euler transformation which carries Σ_i at time 0 into Σ_i at time t, and the angular brackets denote an ensemble average over all equivalent (i) binding sites. In the present work, we use the convention of Rose[48] and Zare[49] for the rotation matrices. An alternative convention is that of Edmonds.[50]

On symmetry grounds we can expect some of the $\langle D^2_{mn} \rangle$ terms appearing in eq 36 to vanish. For chains which bend isotropically with or without intrinsic bends (i.e., with $U^{ba} = 0$ in eq 7), only the $m = n$ terms remain. This is the essence of the "mean cylindrical symmetry" (MCS) approximation.[34] In the present work, however, it can be expected that those

terms with $n = -m$ are nonvanishing as well. In this case, eq 36 reduces to

$$r'(t) = \frac{1}{N-1}\sum_{i=1}^{N-1}\Big[I_0(\epsilon)\,\langle D^2_{00}(\Phi)\rangle + \frac{1}{2}I_1(\epsilon)[\langle D^2_{11}(\Phi)\rangle - e^{2iv}\langle D^2_{1,-1}(\Phi)\rangle + \text{c.c.}] + \frac{1}{2}I_2(\epsilon)\,[\langle D^2_{22}(\Phi)\rangle + e^{4iv}\langle D^2_{2,-2}(\Phi)\rangle + \text{c.c.}]\Big] \quad (38)$$

where "c.c." denotes the complex conjugate of the other terms appearing in the same brackets, $I_0(\epsilon) = (3\cos^2\epsilon/2 - 1/2)^2$, $I_1(\epsilon) = 3\sin^2\epsilon\cos^2\epsilon$, $I_2(\epsilon) = 3\sin^4\epsilon/4$. To date, analytical theories[32−34] have employed the MCS approximation by which the $\langle D^2_{m,-m}\rangle$ terms vanish and eq 38 reduces to

$$r'(t) = \sum_{m=0}^{2} I_m(\epsilon)\, C_m(t)\, F_m(t) \quad (39)$$

where $C_m(t)$ and $F_m(t)$ are twisting and bending correlation functions presented elsewhere.[34,37,38] They contain factors for uniform twisting and tumbling as well as deformational motions. For weakly bending type I models, the $C_m(t)$ and $F_m(t)$ functions can be computed analytically once q, P (or g), R_H, and L are given.

In the analytical theory, it is assumed that torques on the rodlets arising from the torsion potential are fully active but that the *forces* on the beads arising from the torsion potential have a negligible influence on the FPA along an equilibrium trajectory, as recently demonstrated.[20] *At times after all of the twisting deformation modes have relaxed*, one has

$$C_m(t) = B_m(\infty)\, e^{-m^2 D_s^0 t} \quad (40)$$

where D_s^0 is the diffusion constant for uniform azimuthal spinning, and explicit expressions for $B_m(\infty)$ are given elsewhere.[1,22,33−36] Likewise, *at long times after all the bending deformation modes of a weakly bending rod have all relaxed*, one has

$$F_m(t) = D_m(\infty)\, e^{-(6-m^2)D_\perp t} \quad (41)$$

where $D_\perp$ is the rotational diffusion constant for uniform end-over-end tumbling,

$$D_m(\infty) = \frac{1}{2}\sqrt{\frac{\pi}{Z_m}}\,\text{erf}(\sqrt{Z_m})e^{-Z_m/3} \quad (42a)$$

erf denotes the error function, and

$$Z_m = (6 - m^2)L/4P \quad (42b)$$

At sufficiently long times, then D_s^0 and $D_\perp$ are the only quantities in $r'(t)$ that depend on R_H. However, relaxation of the twisting and bending deformations at shorter times also depends upon R_H, so fitting of the *entire* FPA curve to obtain R_H (when q, g (or P_d), and L are known) requires more complete expressions for $C_m(t)$ and $F_m(t)$. Because the Brownian dynamics simulations are not prematurely truncated by the finite lifetime of the chromophore, as happens in real experiments, it is convenient to examine the effective R_H manifested in the FPA via the D_s^0 contribution to $r'(t)$ at long times. In this work, D_s^0 is determined directly from the simulation trajectory according to eq 25, and the simulated FPA curve is then analyzed in terms of the R_H that is inferred from that.

Table 1. Comparison of $X = q\langle(\alpha + \gamma - \phi_0)^2\rangle$ for First- and Second-Order Brownian Dynamics (Torsional) Algorithms[a]

Δt (ns)	X(1st order)	X(2nd order)
0.005	1.010 (0.015)	1.010 (0.006)
0.010	1.022 (0.003)	1.004 (0.006)
0.025	1.038 (0.010)	1.008 (0.012)
0.050	1.082 (0.007)	1.002 (0.014)

[a] Quantities in parentheses denote standard deviations.

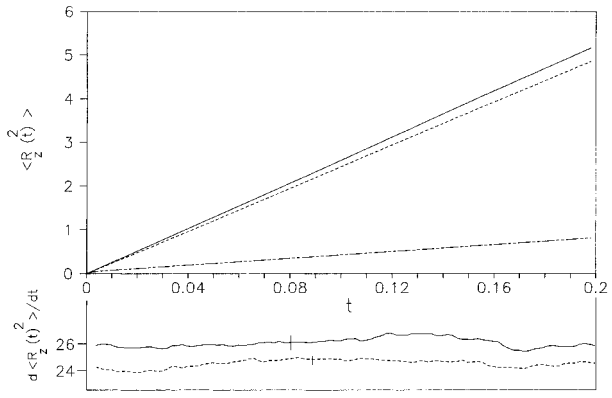

Figure 1. $\langle R_z(t)^2\rangle$ versus t for I-, A-, and L-models. Solid, dashed, and dotted-dashed lines correspond to 10-subunit (72 bp) I-, A-, and L-models, respectively. Time is in microseconds. The bottom insert denotes the time derivatives of the I- and A-models (in microseconds^{-1}).

Results

Test of the First- and Second-Order Algorithms. A useful test of any Brownian dynamics algorithm is to compare quantities such as average bond angles, rms bond lengths, end-to-end distances, end-to-end chain length distributions, etc., obtained from dynamical trajectories with their "starting chain" values.[12] A quantity that is quite sensitive to the dynamics time step is $q\langle(\alpha + \gamma - \phi_0)^2\rangle$ where brackets denote an equilibrium or time average over the $N - 2$ sets of Euler angles. This quantity should equal 1.0. Shown in Table 1 are the results for both first (eq 8) and second (eqs 11−12) order Brownian dynamics (torsional) algorithms for a range of different time steps. The anisotropic (A) model is used ($g = 46.6$, $p = 38.8$, $\beta_0 = 0.273$) with $N = 10$. There is a clear advantage of the second-order algorithm over the first, and the second-order algorithm with a time step of 0.025 ns is used throughout the remainder of this work.

Diffusional "Spinning" of the I-, A-, and L-Models. We consider first the results for 10-bead (72 bp) I-, A-, and L-models. Recall that the I-model has an isotropic bending potential with a straight resting geometry; the A-model has regular anisotropic permanent bends, and the L-model has a single large anisotropic permanent bend (90°) in its middle but otherwise has an isotropic bending potential with a straight resting geometry. Shown in Figure 1 is $\langle R_z^2(t)\rangle$ versus t for these three models. From the long-time slope, it is straightforward to extract D_s^0 given the definition of eq 25. For models I, A, and L, D_s^0 (in 10^{+7} s^{-1}) = 1.321 ± .053, 1.240 ± .024, and 0.196 ± .003, respectively. At the bottom of Figure 1, the time derivative of $\langle R_z^2(t)\rangle$ (in 10^{+6} s^{-1}) for the I- and A- models over the entire time range is also shown (error bars included). For a rigid rod of this length, eq 27 yields $D_{cyl}^{\parallel} = 1.297 \times 10^{+7}$ s^{-1} which agrees with D_s^0 for the I-model within the noise level of the simulations. The results for the

Table 2. D_s^0 versus Chain Length for I- and A-Models[a]

N	D_s^0(I)	D_s^0(A)	D_s^0(A)/D_s^0(I)
4	3.093 (0.049)	2.861 (0.026)	0.925 (0.025)
6	2.145 (0.058)	2.003 (0.051)	0.934 (0.049)
8	1.620 (0.032)	1.519 (0.043)	0.938 (0.048)
10	1.321 (0.053)	1.240 (0.024)	0.939 (0.056)
15	0.894 (0.022)	0.849 (0.026)	0.950 (0.055)
20	0.674 (0.007)	0.614 (0.020)	0.911 (0.043)

[a] D_s^0s are in 10^{+7} s^{-1}. Quantities in parentheses denote standard deviations.

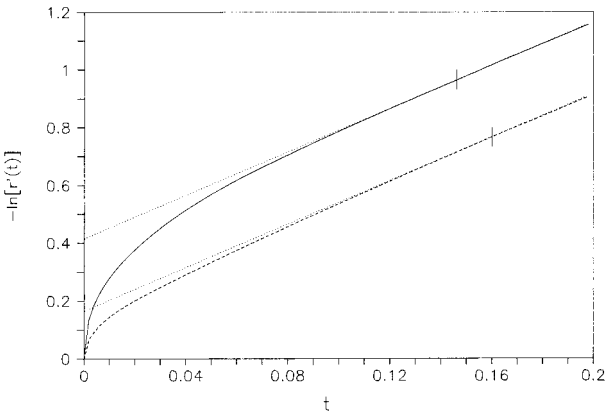

Figure 2. $r'(t)$ versus t for I- and A-models ($\epsilon = 0°$). Solid and dashed lines correspond to 10-subunit (72 bp) I- and A-models. Time is in microseconds. Dotted lines denote the linear fits to the long-time slopes, and short vertical bars denote standard deviations.

L-model confirm that, under certain conditions at least, permanent bends can dramatically reduce the rate of "overall spinning". It should be emphasized, however, that this only occurs when the bend is phase-locked via a large p-parameter at the position of the bend. If the L-model is modified by reducing p from 100 to 0 for bonds 4 and 5 (with all other parameters the same), a D_s^0 comparable to the I model is obtained (data not shown). Although the A-model contains permanent bends that are (partially) phase-locked, the reduction of D_s^0 is much more modest than that for the L-model. Furthermore, the relative reduction appears to be roughly independent of chain length for the regular A-models examined here, as can be seen in Table 2 where simulation results are summarized for N ranging from 4 (28.2 bp) to 20 (144.1 bp). If a ratio of 0.94 is accepted, then anisotropic permanent bending reduces D_s^0 by 6% compared to the I-model. If D_s^0 is equated to $D_{cyl}^{||}$ in eq 27, this corresponds to only a 3% *increase* in effective R_H of the anisotropic permanently bent chain relative to the isotropic case. The negligible variation of D_s^0 (or R_H) with filament length is very likely due to the regular nature of the anisotropic permanent bends in the present model, which might account also for the tiny enhancement of R_H. Whether an appropriate ensemble of random bends would yield a greater variation of R_H with filament length and/or a larger enhancement of R_H is a question that can only be answered by further extensive simulations.

FPA Decays of the I- and A-Models. We next compare the FPA curves of 10-subunit (72 bp) I- and A-models. Plotted in Figure 2 is $-\ln r'(t)$ versus t for the case $\epsilon = 0°$, when the transition dipoles lie along the rodlet z-axes. For this choice of dye geometry, twisting and spinning motions do not contribute to the FPA and the decay is due entirely to bending and overall tumbling. Hence, it is expected that the long-time slopes should approach $6D_\perp$ for both models. Least-squares fitting of the last 30 data points yields $D_\perp = 6.18$ and 6.19×10^5 s^{-1} for cases I and A, respectively. For an ensemble of rigid chains, $D_\perp$ is predicted to be 5.92×10^5 s^{-1}, which is in reasonable agreement with these. It has been our observation that the Brownian dynamics simulations consistently give $D_\perp$'s that are slightly larger than the "rigid ensemble"[44] values. This may be due, at least in part, to a small amount of residual bending contributing to the decay. In fact, if the last 50 (instead of 30) data points are included in the fit, $D_\perp$ comes out around 6.4×10^5 s^{-1}, which is consistent with the notion of residual bending. In any case, the discrepancy between the flexible and rigid chains in regard to $D_\perp$ is small. For both the I- and A-models, the long-time slopes are practically identical, because their rms end-to-end distances are similar. On the other hand, it is clear from the short-time behavior in Figure 2 that there is a much greater amplitude of flexing motions in the I-model than in the A-model, as expected. The dotted lines in Figure 2 represent the straight line fits to the long-time slopes for both I- and A-models. Also, standard deviations are indicated by the vertical bars. Consider first the I-model results. At long times, the reduced anisotropy for $\epsilon = 0°$ should equal $F_0(t)$, which is given by eqs 41 and 42a,b. For $L = 24.49$ nm (corresponding to $N = 10$) and $P = 50$ nm, eq 42a predicts $D_0(\infty) = 0.626$. The ordinate intercept of the straight line fit to the long time slope in Figure 2 corresponds to $-\ln[D_0(\infty)]$, and for the I-model, the simulation yields $D_0(\infty) = 0.657$. In deriving eq 41 and 42, the assumption was made that the rms bending angle between subunits was small. Thus, the small discrepancy between $D_0(\infty)$ obtained by simulation and that computed via eq 41 might be due to the relatively large rms bending angles prevailing in the simulation. In any case, differences between the simulations of the I-model and the analytical expression of Wu et al.[35] are rather small.

It is clear from Figure 2 that it is impossible to find a *simple* I-model that fits the FPA of the A-model. In the simple I-model, for a given L there is a one-to-one correspondence between P and g (eq 34) and, in turn, $D_\perp$.[44] The reason is that $D_\perp$ is very sensitive to the end-to-end distance, which depends on P. Nervertheless, in this case ($\epsilon = 0°$) it is possible to reproduce the A-model results quite well with a hybrid I-model (called the H-model) in which P and $D_\perp$ are regarded as independent parameters. In particular, by taking $D_\perp$ to match the long-time limiting slope of the A-model in Figure 2 and P to match the corresponding ordinate intercept for the A-model in Figure 2, reasonably good agreement with the A-model curve can be obtained. Physically, the long-time slope, or equivalently $D_\perp$, is related to the *static*, or equilibrium, persistence length, while the ordinate intercept is related to the *dynamic* persistence length. From the ordinate intercept (0.17) of the A-model in Figure 2, we get $D_0(\infty) = 0.84$. According to eqs 42a,b, this corresponds to $P_d = 140$ nm. This value is consistent with the experimental findings of Reese[15] on real DNAs. That study was performed using an EPR-active probe whose hyperfine tensor has its principal axis oriented nearly along the DNA. In summary, when $\epsilon = 0°$, a hybrid I-model with $P_d = 140$ nm and $P_{tot} = 50$ nm accounts rather well for the FPA of the A-model.

Most of the FPA experiments performed on DNA have employed ethidium as the extrinsic probe, for which ϵ lies in the range 70−72°. Here, we simply adopt $\epsilon =$

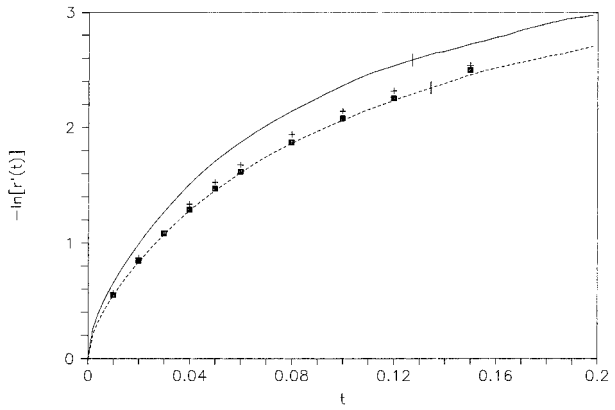

Figure 3. $-\ln[r'(t)]$ versus t for I- and A-models ($\epsilon = 71.9°$). Solid and dashed lines correspond to 10-subunit (72 bp) I- and A-models. The +'s and filled squares represent reconstructed curves using the H-model with $R_H = 1.00$ and 1.03 nm, respectively (see text for details). Time is in microseconds.

71.9°. Consequently, rotations around the local helix axis are sensitively probed. The question arises as to whether an appropriately parametrized H-model could fit the corresponding A-model FPA decay in this case. The H-model FPA is calculated using eq 39 with appropriate choices for $F_m(t)$ and $C_m(t)$. $F_0(t)$ is obtained from a simulation of an I-model with $\epsilon = 0°$ and $P = 140$ nm. It is then multiplied by $\exp[-6(D_\perp - D_\perp')t]$, where $D_\perp'$ is reckoned from its long-time limiting slope and $D_\perp = 6.18 \times 10^5\ s^{-1}$ is reckoned from the long-time limiting slope of the I-model with $\epsilon = 0°$ and $P_d = 50$ nm. This insures that the *deformations* are governed by $P_d = 140$ nm, while the *end-over-end tumbling* reflects $P_{tot} = 50$ nm. Then, the relations $F_1(t) = (F_0(t))^{5/6}$ and $F_2(t) = (F_0(t))^{1/3}$ are employed to approximate $F_1(t)$ and $F_2(t)$.[1] Similarly, $C_n(t)$ is obtained from the results of an I-model simulation using the relation $\ln C_n(t) = -n^2\langle R_z(t)^2\rangle$. Although $C_n(t)$ obtained in this way is independent of the value of P employed in the simulation, it is sensitive to R_H. Simulated $C_n(t)$ curves were obtained using $R = 1.00$ nm and also $R = R_H = 1.03$ nm, which corresponds to the effective hydrodynamic radius that governs diffusional spinning of the A-model. It must be emphasized that $D_\perp$ and $F_n(t)$ are extremely insensitive to such small changes in R_H, but D_s^0 and $C_n(t)$ are very sensitive. Indeed, $D_s^0 \sim R_H^{-2}$. The FPA curves reckoned for the H-model with $R_H = 1.00$ and 1.03 nm are compared with that for an I-model with $P = 50$ nm and $R = 1.00$ nm and with that for the A-model in Figure 3. The H-model with $R_H = 1.03$ nm agrees quite well with the A-model. The FPA curves shown in Figures 2 and 3 were obtained from simulations over 1250 different Brownian dynamics trajectories. A particular simulation, in turn, was broken up into 5 subsimulations of 250 trajectories each, and from the variation in $r'(t)$ or other quantities between subsimulations, standard deviations were estimated. Each trajectory was of 32 000 dynamics steps (800 ns) duration. Under these conditions, standard deviations in $r'(t)$ are quite small. For example, $r'(120\ \text{ns}) = 0.1065 \pm 0.002$ for the A-model with $\epsilon = 71.9°$, which means that the error bars in Figure 3 are comparable to the symbols representing the reconstructed curves.

At least in the case of regular anisotropic permanent bends, such as are exhibited by the present A-model, an appropriately parameterized H-model reproduces the FPA decay of the filament with frozen bends rather well. In particular, provided that (i) $D_\perp$ reflects the end-to-end distance appropriate for $P_{tot} = 50$ nm, (ii) the short-time bending dynamics reflects $P_d = 140$ nm, and (iii) the effective R_H manifested in D_s^0 reflects the enhanced friction for uniform azimuthal rotation of a partially phase-locked fillament, the parametrized H-model agrees rather well with the A-model. This conclusion at least partially validates the use of parametrized I-models in the analysis of experimental FPA data, even though the actual DNA exhibits significant amplitudes of frozen bends. If this same conclusion is eventually found to hold also for random permanent bends, then use of parametrized I-models would be completely justified. That is a topic for future work.

Acknowledgment. J.M.S. acknowledges NSF (MCB-9607344) for partial support of his involvement in this work.

Appendix A: Torques and Forces

The torques and forces acting on the rodlets or subunits have been described previously, but the introduction of the anisotropic bending potential, U^{ba} (eq 7), adds terms to both the torques and forces that were not present before. In addition, it is felt that the present analysis is more general than what has been presented previously and leads to more transparent results. We shall begin with the instantaneous torques.

In the first substep of Brownian dynamics, the subunit positions are held fixed and the rodlets are allowed to rotate about their local z-axes. If δR_{zi} is the displacement of rodlet i, we have from paper I[31]

$$\delta\alpha_i = -\delta R_{zi} \tag{A1a}$$

$$\delta\gamma_i = +\delta R_{zi+1} \tag{A1b}$$

where $i = 1$ to $N - 2$. In this case, $\delta b_i = \delta\beta_i = 0$ and eq 2 becomes

$$\delta U = -\left(\frac{\partial U}{\partial \alpha_1}\right)\delta R_{z1} + \sum_{i=2}^{N-2}\left[\frac{\partial U}{\partial \gamma_{i-1}} - \frac{\partial U}{\partial \alpha_i}\right]\delta R_{zi} + \left(\frac{\partial U}{\partial \gamma_{N-2}}\right)\delta R_{zN-1} \tag{A2}$$

Identifying this with

$$\delta U = -\sum_{i=1}^{N-1} T_i\,\delta R_{zi} \tag{A3}$$

gives the torques on the $N - 1$ rodlets

$$T_1 = \partial U/\partial\alpha_1 \tag{A4a}$$

$$T_i = \frac{\partial U}{\partial \alpha_i} - \frac{\partial U}{\partial \gamma_{i-1}} \quad (i = 2, N-2) \tag{A4b}$$

$$T_{N-1} = -\left(\frac{\partial U}{\partial \gamma_{N-2}}\right) \tag{A4c}$$

From eqs 5 and 7, it is straightforward to show that

$$\frac{T_1}{k_B T} = q(\alpha_1 + \gamma_1 - \phi_0) + p_1\beta_1{}^2(\alpha_1 - \gamma_1 - \psi_{10}) \quad \text{(A5a)}$$

$$\frac{T_i}{k_B T} = q(\alpha_i + \gamma_i - \alpha_{i-1} - \gamma_{i-1}) + p_i\beta_i{}^2(\alpha_i - \gamma_i - \psi_{i0}) + p_{i-1}\beta_{i-1}{}^2(\alpha_{i-1} - \gamma_{i-1} - \psi_{i-10}) \quad (i = 2, N-2) \quad \text{(A5b)}$$

$$\frac{T_{N-1}}{k_B T} = -q(\alpha_{N-2} + \gamma_{N-2} - \phi_0) + p_{N-2}\beta_{N-2}{}^2(\alpha_{N-2} - \gamma_{N-2} - \psi_{N-20}) \quad \text{(A5c)}$$

What is new about eqs A5 is they clearly display the contribution of bending strain to the torques. It should be emphasized however, that only the *anisotropic* bending term contributes.

We shall next turn our attention to the forces on the subunits which are needed in the second Brownian dynamics substep. As discussed in paper I, the subunits are displaced subject to the constraint that the rotations of the rodlets about their local *z*-axes are not allowed. In what follows, we consider a displacement of subunit *i* subject to the constraint that all other subunits are held fixed. Under these conditions the force on subunit *i*, $\mathbf{F}_i$, is related to the virtual change in potential energy by

$$\delta U = -\mathbf{F}_i \cdot \delta \mathbf{r}_i \quad \text{(A6)}$$

Consider first the force that arises from the stretching potential, U^s, which according to eq 3 is independent of the Euler angles. If subunit *i* is displaced while holding all others constant, eq 1 reduces to

$$\delta U^s = \left(\frac{\partial U^s}{\partial b_{i-1}}\right)\delta b_{i-1} + \left(\frac{\partial U^s}{\partial b_i}\right)\delta b_i \quad \text{(A7)}$$

but

$$\delta b_{i-1} = \mathbf{u}_{i-1} \cdot \delta \mathbf{r}_i \qquad \delta b_i = \mathbf{u}_i \cdot \delta \mathbf{r}_i \quad \text{(A8)}$$

and the forces due to stretching are given by

$$\frac{\mathbf{F}_i^s}{k_B T} = h\left[\left(\frac{b_i}{b} - 1\right)u_i - \left(\frac{b_{i-1}}{b} - 1\right)\mathbf{u}_{i-1}\right]$$

If $i = 1$, the $i - 1$ term is omitted, and if $i = N$, the i term is omitted.

The remaining terms for twisting and bending shall be lumped together for the time being. As in the previous example, we shall just displace subunit *i* while holding the others constant, so eq A6 remains valid. The bending and twisting potentials are independent of the b_i's so the first term on the right-hand side of eq 2 does not contribute. As shown in paper I, displacement of subunit *i* causes changes in Euler transformations $\Phi_{i-2,i-1}$, $\Phi_{i-1,i}$, and $\Phi_{i,i+1}$. Thus, it follows that

$$\mathbf{F}_i = -\sum_{j=i-2}^{i}\left[\left(\frac{\partial U}{\partial \alpha_j}\right)\nabla_i\,\delta\alpha_j + \left(\frac{\partial U}{\partial \beta_j}\right)\nabla_i\,\delta\beta_j + \left(\frac{\partial U}{\partial \gamma_j}\right)\nabla_i\,\delta\gamma_j\right] \quad \text{(A9)}$$

When $i = 1$, 2, $N - 1$, or N, j in the above sum is restricted to 1, 1 and 2, $N - 3$ and $N - 2$, or $N - 2$, respectively. In paper I, the changes in Euler angles were related to the virtual rodlet rotations about their local *x*-, *y*-, and *z*-axes. Furthermore, the gradients in these virtual rotations were solved in terms of the $\{\mathbf{f}_i, \mathbf{v}_i, \mathbf{u}_i\}$ vectors. The results are summarized in eq (A10a−i)

$$\nabla_i\,\delta\alpha_{i-2} = \frac{\boldsymbol{\omega}_{i-1}}{b_{i-1}\sin\beta_{i-2}} \quad \text{(A10a)}$$

$$\nabla_i\,\delta\alpha_{i-1} = -\frac{\boldsymbol{\omega}_i}{b_i\sin\beta_{i-1}} + \frac{\boldsymbol{\sigma}_{i-1}\cos\beta_{i-1}}{b_{i-1}\sin\beta_{i-1}} \quad \text{(A10b)}$$

$$\nabla_i\,\delta\alpha_i = -\frac{\boldsymbol{\sigma}_i\cos\beta_i}{b_i\sin\beta_i} \quad \text{(A10c)}$$

$$\nabla_i\,\delta\beta_{i-2} = \boldsymbol{\mu}_{i-1}/b_{i-1} \quad \text{(A10d)}$$

$$\nabla_i\,\delta\beta_{i-1} = -\frac{\boldsymbol{\mu}_i}{b_i} - \frac{\boldsymbol{\zeta}_{i-1}}{b_{i-1}} \quad \text{(A10e)}$$

$$\nabla_i\,\delta\beta_i = \boldsymbol{\zeta}_i/b_i \quad \text{(A10f)}$$

$$\nabla_i\,\delta\gamma_{i-2} = -\frac{\boldsymbol{\omega}_{i-1}\cos\beta_{i-2}}{b_{i-1}\sin\beta_{i-2}} \quad \text{(A10g)}$$

$$\nabla_i\,\delta\gamma_{i-1} = \frac{\boldsymbol{\omega}_i\cos\beta_{i-1}}{b_i\sin\beta_{i-1}} - \frac{\boldsymbol{\sigma}_{i-1}}{b_{i-1}\sin\beta_{i-1}} \quad \text{(A10h)}$$

$$\nabla_i\,\delta\gamma_i = \frac{\boldsymbol{\sigma}_i}{b_i\sin\beta_i} \quad \text{(A10i)}$$

where

$$\boldsymbol{\omega}_i = \sin\gamma_{i-1}\mathbf{f}_i + \cos\gamma_{i-1}\mathbf{v}_i \quad \text{(A11a)}$$

$$\boldsymbol{\sigma}_i = \sin\alpha_i\mathbf{f}_i - \cos\alpha_i\mathbf{v}_i \quad \text{(A11b)}$$

$$\boldsymbol{\mu}_i = \cos\gamma_{i-1}\mathbf{f}_i - \sin\gamma_{i-1}\mathbf{v}_i \quad \text{(A11c)}$$

$$\boldsymbol{\zeta}_i = \cos\alpha_i\mathbf{f}_i + \sin\alpha_i\mathbf{v}_i \quad \text{(A11d)}$$

In what follows, we would like to keep the formulas as general as possible before applying them to specific bending and twisting potentials. Assume that *U* (for bending and/or twisting) can be written as a sum over terms pertaining to individual Euler transformations

$$U^{b,t} = \sum_{k=1}^{N-2} U_k(\alpha_k, \beta_k, \gamma_k) \quad \text{(A12)}$$

Also introduce the notation

$$U_{\alpha j} = \frac{\partial U_j}{\partial \alpha_j}; \quad U_{\beta j} = \frac{\partial U_j}{\partial \beta_j}; \quad U_{\gamma j} = \frac{\partial U_j}{\partial_{\gamma j}} \quad \text{(A13)}$$

Substitution of eqs A10, A12, and A13 into eq A9 leads to ($i = 1$ to $N - 1$)

$$b_i\boldsymbol{\chi}_i = \frac{(U_{\alpha i}\cos\beta_i - U_{\gamma i})\boldsymbol{\sigma}_i}{\sin\beta_i} + \frac{(U_{\alpha i-1} - U_{\gamma i-1}\cos\beta_{i-1})\boldsymbol{\omega}_i}{\sin\beta_{i-1}} + U_{\beta i-1}\boldsymbol{\mu}_i - U_{\beta i}\boldsymbol{\zeta}_i \quad \text{(A14)}$$

where

$$\mathbf{F}_1 = \boldsymbol{\chi}_1 \quad \text{(A15a)}$$

$$\mathbf{F}_j = \boldsymbol{\chi}_j - \boldsymbol{\chi}_{j-1} \quad \text{(A15b)}$$

$$F_N = -\boldsymbol{\chi}_{N-1} \quad \text{(A15c)}$$

When $i = 1$, all $i - 1$ terms in eq A14 are omitted, and when $i = N - 1$, all i terms in eq A14 are omitted. Next consider potential terms of the form

$$U_i^{(\pm)} = f_i(\beta_i)\, h_i(\alpha_i \pm \gamma_i) \quad \text{(A16)}$$

where $f_i(\beta_i)$ and $h_i(\alpha_i \pm \gamma_i)$ are (as yet) unspecified functions of their respective arguments, which have derivatives

$$f_i' = \frac{\partial f_i}{\partial \beta_i} \quad \text{(A17a)}$$

$$h_i' = \frac{\partial h_i}{\partial(\alpha_i \pm \gamma_i)} \quad \text{(A17b)}$$

Substituting eqs A16 and A17 into eq A14 yields

$$b_i\boldsymbol{\chi}_i^{(\pm)} = \mp\left(\frac{1 \mp \cos\beta_i}{\sin\beta_i}\right) f_i h_i'\boldsymbol{\sigma}_i + \left(\frac{1 \mp \cos\beta_{i-1}}{\sin\beta_{i-1}}\right) f_{i-1}h_{i-1}'\boldsymbol{\omega}_i + f_{i-1}'h_{i-1}\boldsymbol{\mu}_i - f_i'h_i\boldsymbol{\zeta}_i \quad \text{(A18)}$$

Equation A18 is sufficiently general to give the forces that arise from isotropic permanent bending (U^{bi}), anisotropic bending (U^{ba}), and twisting (U^{t}). Isotropic bending corresponds to the first term in eq 6, with h_i equal to a constant. Consequently, all h' terms in eq A18 vanish and the isotropic bending contribution to χ^{bi} is

$$b_i\boldsymbol{\chi}_i^{\mathrm{bi}} = g_{i-1}(\beta_{i-1} - \beta_{i-10})\boldsymbol{\mu}_i - g_i(\beta_i - \beta_{i0})\boldsymbol{\zeta}_i \quad \text{(A19)}$$

Anisotropic bending (second term on the right-hand side of eq 7) can be handled by choosing the "−" form of eq A16, but no further simplification in eq A18 can be made. It is straightforward to show that the anisotropic bending contribution is given by

$$b_i\boldsymbol{\chi}_i^{\mathrm{ba}} = \left(\frac{1 + \cos\beta_i}{\sin\beta_i}\right) Q_i\boldsymbol{\sigma}_i + \left(\frac{1 + \cos\beta_{i-1}}{\sin\beta_{i-1}}\right) Q_{i-1}\boldsymbol{\omega}_i + P_{i-1}\boldsymbol{\mu}_i - P_i\boldsymbol{\zeta}_i \quad \text{(A20)}$$

where

$$P_i = k_{\mathrm{B}}Tp_i\beta_i(\alpha_i - \gamma_i - \psi_{i0})^2 \quad \text{(A21a)}$$

$$Q_i = k_{\mathrm{B}}Tp_i\beta_i^2(\alpha_i - \gamma_i - \psi_{i0}) \quad \text{(A22a)}$$

Finally, the contribution of twisting to subunit forces comes from eq 5. The positive form of eq A16 is taken with $f_i = 1$ which means all f' terms in eq A18 vanish. The resulting twisting contributions, χ^{it}, is given by

$$b_i\boldsymbol{\chi}_i^{\mathrm{t}} = -\tan\left(\frac{\beta_i}{2}\right) G_i\boldsymbol{\sigma}_i + \tan\left(\frac{\beta_{i-1}}{2}\right) G_{i-1}\boldsymbol{\omega}_i \quad \text{(A23)}$$

where

$$G_i = q(\alpha_i + \gamma_i - \phi_0) \quad \text{(A24)}$$

Appendix B: Evidence of an Equilibrium between Alternative Secondary Structures

Numerous observations suggest that the average secondary structure of DNA reflects a prevailing equilibrium between two or more alternative conformations with different resting geometries and different torsional and bending rigidities. As would be expected in such a case, those properties that are sensitive to secondary structure, such as the elastic moduli and circular dichroism (CD) spectrum, change significantly in response to practically every conceivable perturbation. First, the torsional and bending rigidities and CD spectra of linearized plasmid DNAs vary substantially with temperature over the premelting region from 5 to 65 °C.[51,52] The observed decline of these torsional rigidities accounts at least in part for the unexpectedly large decrease in supercoiling free energy over this same temperature range.[51] These temperature-induced changes are insensitive to NaCl concentration below 1.0 M, but they are either completely or largely prevented by the addition of 0.5 M tetramethylammonium chloride,[52] which binds preferentially to A·T-rich regions of the DNA.[53] Second, when the NaCl concentration is increased from 1.0 to 5.5 M, the CD spectra of native DNAs undergo a pronounced change from that associated with the canonical 10.4 bp/turn B-helix to that associated with the high-salt 10.2 bp/turn B-helix,[54] and the torsional rigidity decreases substantially.[1,10] Third, inserting a 16 bp $(CG)_8$ sequence near the middle of a 1097 bp restriction fragment from pBR322 has no detectable effect on the tertiary structure, as manifested in the gel mobility and translational diffusion coefficient, but causes a long-range change in the secondary structure, which is manifested by disproportionately large changes (relative to the control DNA without the $(CG)_8$ insert) in the CD spectrum, torsional rigidity, susceptibility to S1 nuclease, and optical melting profile.[10] Conversion of the $(CG)_8$ sequence from B- to Z-DNA between 2.0 and 2.5 M NaCl causes a long-range transition of the flanking DNA to a conformation with substantially greater bending rigidity. In 4.3 M NaCl, binding less than 1 ethidium per 300 bp to this same DNA induces a further extensive change in the secondary structure to a form with a substantially lower bending rigidity and greater CD at 273 nm. In contrast, the control DNA without the $(CG)_8$ insert exhibits no comparable change between 2.0 and 2.5 M NaCl, or upon ethidium binding in 4.3 M NaCl. Fourth, in 0.01 M NaCl, variations in the superhelix density cause extensive changes in the secondary structure, as manifested in the torsional rigidity, CD spectrum, and dynamic light scattering at large scattering vector.[8,9,11] Fifth, imposing a permanent bending strain by circularizing small DNAs with fewer than 250 bp shifts the secondary structure equilibrium toward a state with a substantially (1.4- to 1.9-fold) larger torsional rigidity, an appreciably enhanced intrinsic binding constant for ethidium, an altered CD spectrum, and presumably also

a greater permanent bend.[55] Responses of linear and supercoiled DNAs to other kinds of perturbations are detailed elsewhere.[1]

The long-range or extensive character of some of these changes indicates that the average size of the secondary structure domains can be surprisingly large, extending to at least several hundred base pairs.[10] The extremely slow kinetics of observed changes subsequent to variations in temperature,[10] salt concentration,[10] superhelix density,[1,8,9,11] and bending[55] is consistent with a very large cooperativity of these structural changes.

The extent of "permanent" bending also seems to reflect a balanced equilibrium between bent and straight, or at least straighter, states of DNA. The degree of permanent bending, as monitored by anomalous gel mobility, decreases with increasing temperature and disappears altogether between 60 and 65 °C.[56,57] In addition, alcohols diminish the bending associated with oligoA tracts,[58] whereas Mg^{2+} ions enhance the bends of GGGCCC and certain other sequences.[56,59,60] Moreover, the force vs extension curves for single very long DNA molecules are fitted extremely well, even near full-length extension, by a simple wormlike chain version of model I with $P = 50$ nm, which takes no account of any permanent bends.[61,62] This suggests that moderate tension (below that required for full extension) may also shift the secondary structure equilibrium in favor of intrinsically straight states. Model I with $P = 50$ nm also appears to account adequately for the off-field decays of the transient electric dichroism and birefringence on the microsecond time scale.[24] However, that conclusion is contingent on the validity of two extra assumptions, namely, that the DNA configurations are not altered by the applied electric field and that the distorted ion atmosphere does not contribute to the relaxation, which might not hold under the prevailing experimental conditions. For whatever reason, the results suggest that any effects of permanent bends are substantially diminished in these electrooptic experiments. If changes in the extent of permanent bending are caused by shifts in the secondary structure equilibrium between bent and straight(er) conformations, as some of these experiments indicate, then imposing a permanent bending strain should alter the secondary structure equilibrium. Indeed, that is precisely what was found,[55] as noted above.

References and Notes

(1) Schurr, J. M.; Fujimoto, B. S.; Wu, P.; Song, L. In Topics in Fluorescence Spectroscopy, Vol. 3: Biochemical Applications, J. R., Lakowicz, Ed.; Plenum Press: New York, 1992; pp 137−229.
(2) Schurr, J. M.; Schmitz, K. S. *Annu. Rev. Phys. Chem.* **1986**, *37*, 271.
(3) Hagerman, P. J. *Annu. Rev. Biophys. Biophys. Chem.* **1988**, *17*, 265.
(4) Taylor, W. H.; Hagerman, P. J. *J. Mol. Biol.* **1990**, *212*, 363.
(5) Landau, L. D.; Lifschitz, E. M. *Statistical Physics*; Pergamon Press: New York, 1969; section 151.
(6) Schellman, J. A.; Harvey, S. C. *Biophys. Chem.* **1995**, *55*, 95.
(7) Heath, P. J.; Clendenning, J. B.; Fujimoto, B. S.; Schurr, J. M. *J. Mol. Biol.* **1996**, *260*, 718.
(8) Song, L.; Fujimoto, B. S.; Wu, P.; Thomas, J. C.; Shibata, J. H.; Schurr, J. M. *J. Mol. Biol.* **1990**, *214*, 307.
(9) Wu, P.; Fujimoto, B. S.; Song, L.; Schurr, J. M. *Biophys. Chem.* **1991**, *41*, 217.
(10) Kim, U. S.; Fujimoto, B. S.; Furlong, C. E.; Sundstrom, J. A.; Humbert, R.; Teller, D. C.; Schurr, J. M. *Biopolymers* **1993**, *33*, 1725.
(11) Naimushin, A. N.; Clendenning, J. B.; Kim, U. S.; Song, L.; Fujimoto, B. S.; Stewart, D. W.; Schurr, J. M. *Biophys. Chem.* **1994**, *52*, 219.
(12) Allison, S. A.; Austin, R. H.; Hogan, M. *J. Chem. Phys.* **1989**, *90*, 3843.
(13) Song, L.; Schurr, J. M. *Biopolymers* **1990**, *30*, 229.
(14) Hustedt, E. J.; Spaltenstein, A.; Kirchner, J. E.; Mailer, C.; Hopkins, P. B.; Robinson, B. H. *Biochemistry* **1993**, *32*, 1774.
(15) Reese, A. Ph.D. Thesis, University of Washington, Seattle, WA, 1996.
(16) Fujimoto, B. S.; Schurr, J. M. *Nature* **1990**, *344*, 175.
(17) Gebe, J. A.; Allison, S. A.; Clendenning, J. B.; Schurr, J. M. *Biophys. J.* **1995**, *68*, 619.
(18) Gebe, J. A.; Delrow, J. J.; Heath, P. J.; Stewart, D. W.; Schurr, J. M. *J. Mol. Biol.* **1996**, *262*, 105.
(19) Schurr, J. M.; Fujimoto, B. S.; Reese, A.; Robinson, B. H.; Allison, S. A. *J. Chem. Phys.* **1997**, *106*, 815.
(20) Heath, P. J.; Allison, S. A.; Schurr, J. M. *Macromolecules* **1996**, *29*, 3583.
(21) Collini, M.; Chirico, G.; Baldini, G. *J. Chem. Phys.* **1996**, *104*, 6058.
(22) Fujimoto, B. S.; Miller, J. M.; Ribeiro, N. S.; Schurr, J. M. *SPIE Proc.* **1994**, *1922*, 360.
(23) Fujimoto, B. S.; Schurr, J. M. *Biophys. J.* **1995**, *68*, A101.
(24) Allison, S. A.; Nambi, P. *Macromolecules* **1992**, *25*, 759.
(25) Allison, S. A.; McCammon, J. A. *Biopolymers* **1984**, *23*, 363.
(26) Allison, S. A. *Macromolecules* **1996**, *19*, 118.
(27) Song, L.; Allison, S. A.; Schurr, J. M. *Biopolymers* **1990** *29*, 1773.
(28) Heath, P. J.; Allison, S. A.; Gebe, J. A.; Schurr, J. M. *Macromolecules* **1995**, *28*, 6600.
(29) Chirico, G.; Langowski, J. *Macromolecules* **1992**, *25*, 769.
(30) Chirico, G.; Langowski, J. *Biopolymers* **1994**, *34*, 415.
(31) Chirico, G.; Langowski, J. *Biophys. J.* **1996**, *71*, 955.
(32) Barkley, M. D.; Zimm, B. H. *J. Chem. Phys.* **1979**, *70*, 2991.
(33) Allison, S. A.; Schurr, J. M. *Chem. Phys.* **1979**, *41*, 35.
(34) Schurr, J. M. *Chem. Phys.* **1984**, *84*, 71.
(35) Wu, P.-G.; Fujimoto, B. S.; Schurr, J. M. *Biopolymers* **1987**, *26*, 1463.
(36) Schurr, J. M.; Fujimoto, B. S. *Biopolymers* **1988**, *27*, 1543.
(37) Nuutero, S.; Fujimoto, B. S.; Flynn, P. F.; Reid, B. R.; Ribeiro, N. S.; Schurr, J. M. *Biopolymers* **1994**, *34*, 463.
(38) Fujimoto, B. S.; Miller, J. M.; Ribeiro, N. S.; Schurr, J. M. *Biophys. J.* **1994**, *67*, 304.
(39) Schurr, J. M. *Bioplymers* **1985**, *24*, 1023.
(40) Iniesta, A.; Garcia de la Torre, J. *J. Chem. Phys.* **1990**, *92*, 769.
(41) Ermak, D.; McCammon, J. A. *J. Chem. Phys.* **1978**, *69*, 1352.
(42) Eimer, W.; Pecora, R. *J. Chem. Phys.* **1991**, *94*, 2324.
(43) Diaz, R.; Fujimoto, B. S.; Schurr, J. M. *Biophys. J.* **1997**, *72*, A322.
(44) Hagerman, P. J.; Zimm, B. H. *Biopolymers* **1981**, *20*, 1481.
(45) Hagerman, P. J. *Biopolymers* **1981**, *20*, 1503.
(46) Tirado, M. M.; Garcia de la Torre, J. *J. Chem. Phys.* **1980**, *73*, 1986.
(47) Smith, S. B.; Cui, Y.; Bustamante, C. *Science* **1996**, *271*, 795.
(48) Rose, M. E. *Elementary Theory of Angular Momentum*; John Wiley & Sons: New York, 1957.
(49) Zare, R. N. *Angular Momentum*; John Wiley & Sons, New York, 1988.
(50) Edmonds, A. R. *Angular Momentum in Quantum Mechanics*; Princeton University Press: Princeton, NJ, 1974.
(51) Delrow, J. J.; Heath, P. J.; Schurr, J. M. On the Origin of the Temperature Dependence of the Supercoiling Free Energy. *Biophys. J.* 1997, in press.
(52) Delrow, J. J.; Heath, P. J.; Schurr, J. M. *Biophys. J.* **1997**, *72*, A322.
(53) Shapiro, J. T.; Stannard, B. S.; Felsenfeld, G. *Biochemistry* **1969**, 8, 233.
(54) Baase, W. A.; Johnson, W. C., Jr. *Nucleic Acids Res.* **1979**, *6*, 797.
(55) Heath, P. J.; Clendenning, J. B.; Fujimoto, B. S.; Schurr, J. M. *J. Mol. Biol.* **1996**, *260*, 718.
(56) Diekmann, S. *Nucleic Acids Res.* **1987**, *15*, 247.
(57) Chan, S. S.; Breslauer, K. J.; Hogan, M. E.; Kessler, D. J.; Austin, R. H.; Ojemann, J.; Passner, J. M.; Wiles, N. C. *Biochemistry* **1990**, *29*, 6161.
(58) Sprous, D.; Zacharias, W.; Wood, Z. A.; Harvey, S. C. *Nucleic Acids Res.* **1995**, *23*, 1816.
(59) Brukner, I.; Susic, S.; Dlakic, M.; Savic, A.; Pongor, S. *J. Mol. Biol.* **1994**, *236*, 26.
(60) Dlakic, M.; Harrington, R. E. *J. Biol. Chem.* **1995**, *270*, 29945.
(61) Bustamante, C.; Marko, J.-F.; Siggia, E. D.; Smith, S. *Science* **1994**, *265*, 1599.
(62) Wang, M. D.; Yin, H.; Landick, R.; Gelles, J.; Block, S. M. *Biophys. J.* **1997**, *72*, 1335.

MA970877R